Redox Biology 36 (2020) 101622

Contents lists available at ScienceDirect

Redox Biology

journal homepage: www.elsevier.com/locate/redox

KLF2 regulates dental pulp-derived stem cell differentiation through the induction of mitophagy and altering mitochondrial metabolism

Jyotirindra Maity, Moonmoon Deb, Carl Greene, Hiranmoy Das *

Department of Pharmaceutical Sciences, Jerry H. Hodge School of Pharmacy, Texas Tech University Health Sciences Center, Amarillo, TX, USA

ARTICLE INFO

Keywords:
Autophagy
DPSC
Histone acetylation
Histone methylation
KLF2
Mitophagy
OB differentiation

ABSTRACT

To define the regulatory role of Kruppel-like factor 2 (*KLF2*) during osteoblast (OB) differentiation of dental pulp-derived stem cell (DPSC)s, herein, we show that the levels of KLF2 and autophagy-related molecules were significantly increased in differentiated cells. Gain-of-function and loss-of-function approaches of *KLF2* confirmed that *KLF2* modulated autophagic and OB differentiation-related molecules. In addition, knockdown of the autophagic molecule (*ATG7* or *BECN1*) in DPSCs resulted in reduced levels of KLF2 and OB differentiation-related molecules. Conversely, the induction of autophagy increased levels of KLF2 and OB differentiation-related molecules. Moreover, OB differentiation induced mitophagy and mitochondrial membrane potential-related molecules. In addition, OB differentiation reduced the generation of total and mitochondrial ROS productions and induced intracellular Ca^{2+} production. Measurements of glycolysis and oxidative phosphorylation simultaneously in live cells revealed that OB differentiation decreased the oxygen consumption rate, which is an indicator of mitochondrial respiration and reduced the level of ATP production. Furthermore, flux analysis also revealed that OB differentiation increased the extracellular acidification rate (ECAR) in the non-glycolytic acidification, and the glycolytic capacity conditions, increasing the lactate production and reducing the metabolic activity of the cells. Thus, a metabolic shift from mitochondrial respiration to the glycolytic pathway was observed during OB differentiation. Finally, chromatin immunoprecipitation (ChIP) analysis confirmed that the *KLF2* and active epigenetic marks (H3K27Ac and H3K4me3) were upregulated in the promoter region of *ATG7* during OB differentiation. These results provide evidence that the mitophagy process is important during OB differentiation, and *KLF2* critically regulates it.

1. Introduction

Osteoblast (OB)s are terminally differentiated specialized cells that originate from mesenchymal stem cell (MSC)s, form bones for maintaining bone homeostasis, and dysregulation of this process causes bone pathogenesis [1]. The orchestrated process of OB differentiation mainly involves the formation of intracellular proteins, mineralization of the cytoskeleton structure, and changes in the intracellular organelles of the cells [2]. However, the regulatory mechanism of OB formation from stem cells remains elusive. MSCs are multipotent precursors, capable of differentiating into various lineages, including osteocytes, adipocytes, cardiomyocytes, and neurons when exposed to the appropriate signals [3]. The human dental pulp contains precursor cells known as dental pulp stem cells (DPSC) also exhibit self-renewal and multilineage differentiation abilities, and shares phenotypic and morphological characteristics with MSCs. Osteogenic differentiation of DPSCs can be achieved upon stimulation with a phytoestrogen, ferutinin by modulating Wnt/β-catenin signaling as recently demonstrated [4].

Autophagy, specifically macroautophagy is an evolutionarily conserved intracellular catabolic process, which degrades unwanted cellular proteins and damaged or excess organelles from the cells [5]. There are three types of autophagy, such as, chaperon-mediated autophagy, microphagy and macrophagy, helping in maintaining cellular homeostasis by clearing intracellular garbage [6]. Accumulating data suggest that autophagy plays a major role in cellular aging [7,8], and various pathological conditions including cancers, heart and neurodegenerative diseases [9]. These pathological conditions are caused mainly due to the imbalances in engulfing long-lived proteins and damaged organelles within the cells [10]. We recently showed that autophagy is involved in osteoclastogenesis process, which is regulated by a transcriptional factor, KLF2 [11]. The study suggests that

* Corresponding author. Department of Pharmaceutical Sciences, Jerry H. Hodge School of Pharmacy, Texas Tech University Health Sciences Center, ARB Suite 2116, National Academy of Inventors, 1406 South Coulter Street, Amarillo, TX, USA.
E-mail address: hiranmoy.das@ttuhsc.edu (H. Das).

https://doi.org/10.1016/j.redox.2020.101622
Received 15 May 2020; Received in revised form 19 June 2020; Accepted 24 June 2020
Available online 3 July 2020

Abbreviations

Ad-*KLF2* adenoviral construct of *KLF2*
ATG3 autophagy related 3
ATG5 autophagy related 5
ATG7 autophagy related 7
BECN1 beclin1, autophagy related
BGLAP/osteocalcin bone gamma-carboxyglutamate protein
ChIP chromatin immunoprecipitation
DCFDA 2′,7′-Dichlorodihydrofluorescein diacetate
EV empty vector
ECAR extracellular acidification rate
JC1 5,5′,6,6′-Tetrachloro-1,1′,3,3′-tetraethylbenzimidazolylcarbocyanine iodide
H3K27Ac histone H3 lysine 27 acetylation
H3K4me3 histone H3 lysine 4 trimethylation
KLF2 kruppel-like factor 2 (lung)
MAP1LC3B/LC3B microtubule-associated protein 1 light chain 3 beta
MDC monodansylcadaverine
mTOR mammalian target of rapamycin
NS non-specific
OCR oxygen consumption rate
PCR polymerase chain reaction
PtdIns3K phosphoinositide 3-kinase
si*KLF2* small interfering KLF2 ribonucleic acid
SPARC/osteonectin secreted protein acidic and cystine rich
SPP1/osteopontin secreted phosphoprotein 1
TSS transcriptional start site
UCSC University of California, Santa Cruz

autophagy also plays a crucial role in OB differentiation involving mineralization and bone homeostasis process [12]. However, the role of KLF2 in this process is yet to be defined.

Mitochondria are the powerhouse of the cells and very dynamic organelles, which fuse and divide during the life cycle of a cell [13]. Mitochondria are critically important organelles in cells and their function, quantity, and quality are necessary for the maintenance of cellular survival. Cells maintain a healthy mitochondrial network by employing many quality control pathways. Among them, mitochondrial chaperones protect polypeptides by helping in their protein folding during transportation into the mitochondria [14]. If any misfolding of the protein occurs, mitochondrial proteases eliminate the proteins [15]. Simultaneously, damaged mitochondrial components are sequestered and/or diluted through mitochondrial fission and fusion processes [16]. Cells preserve a healthy mitochondrial population in daughter cells by asymmetrical apportioning of mitochondria during cell division [17,18]. However, if mitochondria are damaged beyond repair, mitochondria are engulfed with autophagosomes and degraded through the mitophagy process [19].

Various biosynthetic pathways, ATP production, Ca^{2+} buffering, and apoptotic signaling, which are critically regulated by mitochondria, and damaged mitochondria severely affect those functions [20]. Reactive oxygen species (ROS), which are produced as byproducts of normal oxidative phosphorylation in mitochondria [21], regulate cell differentiation, growth, aging, and cell death [22]. Small elevation in the level of ROS production activates cell signaling pathways to elicit antioxidant responses to protect cells against severe damage [23]. Multiple enzymes react with reactive oxygen species to reduce their numbers to protect any damage to DNA, proteins, and lipids present in mitochondria [22]. It was shown that mild oxidative stress activates transcription of the PINK1 molecule [24] and initiates the mitophagy process [25].

Kruppel-like factors (KLFs) belong to the members of zinc finger transcription factors, and at least 17 mammalian family members of the KLFs are currently identified [26]. KLF2 is one of the important members of the KLF family, which was first identified as a critical regulator for normal lung development [27]. Later it was revealed that it has implications in many important biological processes, such as T cell migration [28], embryonic erythropoiesis [29], vascular integrity [30], and monocyte activation, function, and differentiation [11,31–34]. Studies suggest that KLF2 is essential for maintaining ground state pluripotency of mouse embryonic stem cells [35], differentiation of endothelial progenitor cells to endothelial cells induced by shear stress [36]. It is apparent that the expression of KLF2 is decreased in various cellular differentiation processes, such as activation in myeloid cells [31], activation in endothelial cells [37], and osteoclast differentiation of myeloid cells [11]. However, functions and regulation mechanisms of KLF2 during OB differentiation of DPSC are yet to be established. The current study was undertaken to define the role of KLF2 in regulating autophagy/mitophagy-mediated osteoblastogenesis processes in human DPSCs.

2. Materials and methods

2.1. Reagents and antibodies

Human dental pulp derived stem cells (DPSC) were isolated from discarded third molar teeth, which were obtained after surgical extraction from a healthy adolescent donor with prior approval from the Institutional Review Board (IRB) and consent from the donors. Imprint Chromatin Immunoprecipitation kit (17–295), Minimum Essential Medium (MEM, M8042-500 ML), Dulbecco's Modified Eagle's Medium (DMEM, D6429-500 ML), Trypsin (25200-056), L-Ascorbic Acid (LAA, A92902), monodansylcadaverine (MDC, D4008), Rapamycin (R0395), 37% Paraformaldehyde (252549), Ponceau (P7170), TEMED (161–800), JC1 dye (T3168), DCFDA (D6883), fluoro 4 (F14201) were obtained from Sigma-Aldrich Corporation. Fixative for TEM (15960-01) was from Electron microscopy sciences. Seahorse XF cell mito-stress kit (103035-100), Glycolysis stress kit (103020-100), XF Base Medium (102353-100), XF calibrant (100840-000), Glucose Solution (103577-100), Pyruvate Solution (103578-100), Glutamine Solution (103579-100) were purchased from Agilent. Bradford reagent (500-0006) was from Bio-Rad. 4% Paraformaldehyde (sc-281692) was from Santa Cruz. Hanks' balanced salt solution (HBSS, 21-020-CV) was from Mediatech Inc. The si*ATG7* (AM16708), si*BECN1* (4457298), negative control si*RNA* (AM4611), si*KLF2* (4392420) and DEPC-Treated Water (AM9922) were purchased from Ambion. Alizarin Red Solution (2003999) was obtained from Chemicon international. β Glycerophosphate (157241) was obtained from MP biomedical. Opti-MEM (31985), FBS (10438-026), PBS (70013-032), L-Glutamine (25030), Pen strep (10378-016), Anti-Anti (15240), Mitosox red (M36008), TRIzol reagent (15596026), cDNA kit (4387406), Lipofectamine 2000 (11668019) and mounting medium (P10144) were purchased from Invitrogen Corporation. SYBR Green PCR Kit (4309155) was from Applied Biosystem. Protogel (EC-890) was from National diagnostics. BSA (BP1600-100), 20% SDS (BP1311-1), DMSO (BP231-100), NaOH (1310-73-2497-19-8), Methanol (A412P-4) were from Fisher scientific. Separating buffer (BP-90), Stacking buffer (BP-95), Running buffer (BP-150), Transfer buffer (BP-190), TBS-T (IBB-180) were from Boston Bioproducts. Non-fat dry milk (M0841) was obtained from LabScientific. Antibodies for BECN1 (3738S), ATG3 (3415S), ATG5 (12994S), ATG7 (8558S), LC3B (2775), mTOR (2972S), Wnt5a (2530T), β-catenin (9562S), DVL3 (3218T), LRP6 (3395T), RUNX2 (8486S), osteonectin

(8725S) and GAPDH (2118S), mitophagy related protein PINK1 (6946S), Parkin (2132S), Anti-mouse IgG, HRP-linked Antibody (7076), Anti-rabbit IgG, HRP-linked Antibody (7074) were purchased from Cell Signaling Technology. RIPA lysis buffer (20–188) and antibody for osteocalcin (AB10911) were purchased from Millipore. Osterix (ab94744), osteopontin (ab8448), H3K4me3 (ab1012), H3K27Ac (ab4729), KLF2 (ab203591), goat IgG (ab37373) were purchased from Abcam.

2.2. Cell lines and culture conditions

Primary dental pulp stem cells (DPSC), were cultured in alpha MEM with 20% FBS, 1% penicillin-streptomycin. All cells were maintained at 37 °C, 5% CO_2, and 95% relative humidity. Primary DPSCs were used between passages 3–9. DPSC starvation was performed by incubating exponential growing cells in Hank's balanced salt solution (HBSS).

2.3. OB differentiation

DPSC cells were cultured in αMEM supplemented with 20% fetal bovine serum (FBS) (10438-026) and 100 U ml^{-1} penicillin-streptomycin (15140-122) all from GIBCO, Thermo Fisher Scientific, incubated in 5% CO_2 at 37 °C. Cells were harvested and sub-cultured according to experimental requirements. To induce OB differentiation, DPSC cells were cultured in DMEM containing 10% heat-inactivated FBS in the presence of β-glycerophosphate (BGP, 10 mM final concentration) + L-Ascorbic acid (LAA, 60 μM final concentration). The fresh medium was replaced every third day of culture.

2.4. Alizarin Red staining

Alizarin red staining was used to detect differentiated OB cells following the manufacturer's protocol. Briefly, DPSCs were cultured on a 6-well plate for differentiation into OBs in the presence or absence of BGP + LAA for 14 days. Cells were fixed with 4% paraformaldehyde in 1 x PBS for 20 min at various time points, at room temperature, and then washed with 1 x PBS for 3 times. Next, Alizarin red stain was applied on each plate equally and incubated for 30 min at 37 °C protected from light. Finally, the plate wells were rinsed with deionized water for at least 3 times and then examined under a light microscope, (Olympus Corporation of the Americas, Waltham, MA, ix81).

2.5. MDC staining

To determine the presence of autophagic vesicles in OB differentiated cells as well as control cells, DPSCs were grown on sterile coverslips inserted into a 6-well plate and induced to differentiate into OBs with BGP + LAA or cultured untreated. In addition, to confirm the effect of *KLF2* on the formation of an autophagic vesicle, we infected DPSCs with an adenoviral overexpression approach (Ad-*KLF2*) and knocked down of *KLF2 in DPSCs* using siRNA transfection method. During the course of differentiation, at various time points such as days 1, 3, 7, and 14, cells were stained with auto-fluorescent compound MDC dye following the manufacturer's protocol. In brief, cells were incubated with 50 mmol/L concentration of MDC at 37 °C for 15 min and washed with 1 x PBS for three times. Finally, the cells were mounted on a glass slide, viewed under a fluorescence microscope (Olympus Corporation of the Americas, Waltham, MA, Slide book 5.0 × 64 software ix81), and images were captured digitally.

2.6. JC1 staining

DPSC cells (2×10^4) were seeded in a 35 mm plate for overnight. After 16 h, cells were treated with BGP + LAA for 7 days. The cells were then washed with 1 x PBS thrice and incubated with JC1 dye for 20 min at 37 °C. After washing with 1 x PBS, the cells were mounted on glass slides and viewed under a fluorescence microscope (Olympus Corporation of the Americas, Waltham, MA, Slide book 5.0 × 64 software ix81).

2.7. ROS measurement

Reactive oxygen species (ROS) measurement was performed by using 2′,7′- dichlorodihydrofluorescein diacetate (DCFDA, 4091-99-0, Sigma Aldrich, USA) that enters into the cells and interacts with a reactive oxygen molecule to generate a green fluorescent compound dichlorodihydrofluorescein (DCF). Briefly, a stock solution of DCFDA (10 mM) was prepared in methanol and was further diluted with culture medium to a working solution of 100 μM concentration. DPSCs (2×10^4) were seeded in a 10 cm plate for overnight. After 16 h, cells were treated with BGP + LAA for 14 days for osteoblast differentiation. Control DPSCs were cultured for 14 days with a culture medium (α-MEM). After differentiation of cells or undifferentiated cells were washed with ice-cold Hank's balanced salt solution and incubated with 100 μM (working solution) of DCFDA for 30 min at 37 °C. Then, cells were lysed with 0.1 M NaOH alkaline solution and fluorescence intensity was measured using a plate reader (Synergy 2, BioTek Instruments, Inc, Winooski, USA) at a setting excitation of 495 nm and emission at 529 nm using 200 μl/well of lysate. Each experiment was performed at least three times and used triplicate for each assay.

2.8. Mitochondrial superoxide measurement

Mitochondrial superoxide production was evaluated by the mitosox red compound (M36008, Thermo Fisher Scientific, USA). Oxidation of mitosox red by superoxide compounds present in mitochondria produces red fluorescence. In brief, we prepared a 5 mM stock solution of mitosox in DMSO. DPSCs (2×10^4) were seeded in a 10 cm dish overnight. After 16 h, cells were treated with BGP + LAA for 14 days for osteoblast differentiation. Control cells were cultured for 14 days with a culture medium (α-MEM). After differentiation of cells or undifferentiated cells were washed with ice-cold 1 x PBS and incubated with 2 μM (working solution) of mitosox red for 30 min at 37 °C. Then, cells were harvested through scrapping and fluorescence intensity was measured using a plate reader (Synergy 2, BioTek Instruments, Inc, Winooski, USA) at a setting excitation of 510 nm and emission at 580 nm using 200 μl/well of lysate. Each experiment was performed at least three times and used triplicate for each assay.

2.9. Intercellular calcium (Ca^{2+}) measurement

Intracellular Ca^{2+} was measured using a fluor 4 compound (A20173, Thermo Fisher Scientific). A stock solution of 1 nM in DMSO was prepared. DPSCs (2×10^4) were seeded in a 10 cm dish overnight. After 16 h, cells were treated with BGP + LAA for 14 days for osteoblast differentiation. Control cells were cultured for 14 days with a culture medium (α-MEM). Cells were washed with ice-cold 1 x HBSS three times and incubated with 3 μM (working solution) of fluor 4 for 30 min at 37 °C. Cells were then washed with HBSS three times. After differentiation, or undifferentiated cells were harvested through scrapping after lysing with 0.1 M NaOH alkaline solution and fluorescence intensity was measured using a plate reader (Synergy 2, BioTek Instruments, Inc, Winooski, USA) at a setting at excitation of 488 nm and emission at 520 nm using 200 μl/well of lysate. Each experiment was performed at least three times and used triplicate for each assay.

2.10. Western blot analysis

Western blot was performed to determine the levels of the various autophagic proteins like ATG7, ATG5, ATG3, BECN1, and LC3B; OB marker proteins like RUNX2, SPARC, BGLAP, SPP1; signaling protein like Wnt5a, β-catenin, DVL3, LRP6 along with KLF2. GAPDH was used as an internal control in DPSC cells during the course of differentiation. The

cells were lysed in 60 μl pre-cooled RIPA lysis buffer (Millipore Sigma Aldrich Corporation, 20–188) for 20 min on ice and centrifuged at 13,200×*g* for 15 min. The supernatant was collected and protein concentration was estimated with Bradford's reagent (Bio-Rad Incorporation, 5000006) using bovine serum albumin (BSA) (Sigma Aldrich Corporation, A7906-10G) as a standard. Equal amounts of protein (40 μg) were separated by 10–12% SDS-PAGE gels electrophoretically and transferred to polyvinylidene difluoride membrane (Bio-Rad Incorporation, 1620115). After blocking with 5% BSA for 1 h at room temperature, the membranes were incubated with primary antibodies for 12–16 h at 4 °C. Then membranes were re-incubated with appropriate HRP (horseradish peroxidase)-labeled secondary antibodies (Cell Signaling Technology, 7074, and 7076) for 1 h at room temperature. Immunoreactive protein bands were visualized by enhanced chemiluminescence (ECL, Amersham Pharmacia Biotechnology, RPN2232), and the band detections were performed within the linear range.

2.11. Overexpression and knockdown of KLF2

KLF2 overexpression was induced in DPSC cells using adenoviral constructs of *KLF2* (Ad-*KLF2*, used 1:100 MOI), empty vector (EV) as control. The plasmids were generated by the Harvard Gene Therapy Initiative (Harvard Medical School, Boston, MA, a kind gift from Mukesh K. Jain, Case Western Reserve University, Cleveland), in the presence of polybrene (Millipore Sigma Aldrich Corporation, 107689, final concentration, 8 ng/ml), as described in our earlier studies [31]. On the other hand, *KLF2* knockdown was performed with *KLF2* sequence-specific siRNA, keeping non-specific siRNA as control (Dharmacon Incorporation), and transfected with Lipofectamine 2000 (Thermo Fisher Scientific, 11668019) using 60 nmol/L concentrations as described earlier [31].

2.12. RNA extraction and real-time PCR

Total RNA was extracted by TRIzol reagent (Invitrogen Corporation, 15596026), and cDNA was prepared using the PrimeScript reverse transcription kit according to the manufacturers' protocols. Real-time PCR amplification reactions were performed with the SYBR Green PCR Kit (Applied Biosystem, 4309155). The relative expression of the target gene was quantified by calculating Ct (threshold cycle) values and normalized by *β-Actin* levels. Each sample was analyzed in a triplicate manner. We used the primer sets of genes described in Table- S1 that were purchased from Sigma Aldrich Corporation.

2.13. Chromatin immunoprecipitation (ChIP) and quantitative PCR

ChIP analysis was performed by using Imprint® Chromatin Immunoprecipitation Kit (Sigma Aldrich Corporation, CHP1 96RXN) following manufacturers' protocol. In brief, after chromatin cross-linking with 1% formaldehyde and DNA shearing, chromatin-protein complexes were immunoprecipitated from BGP + LAA-treated DPSCs, compared to undifferentiated DPSCs (control) with antibodies against KLF2 (Abcam, ab203591), H3K27Ac (Abcam, ab4729), and H3K4me3 (Abcam, ab1012). Antibody against goat IgG (Abcam, ab37373) was used as a negative control. The quantitative PCR analysis was performed with the selected primers from the transcriptional start sites of the *ATG7* promoter regions (Fig. S1), and the primer sequences were described in Table- S2. Values obtained from the ChIP assay were normalized with background obtained from the precipitation with respective control antibodies. Percent (%) input was analyzed using the standard formula. Each experiment was performed in triplicate at least 3 times.

2.14. Transmission electron microscopy (TEM)

DPSCs were treated with BGP + LAA for 14 days in DMEM complete medium or cultured in DMEM complete medium only. Cells were then collected and prefixed with 2.5% glutaraldehyde. These cells were then post-fixed with 1% osmium tetra-oxide for 1 h in dark. Cells were then dehydrated by increasing concentrations of acetone. These cells were then embedded with epoxy resin. Polymerization of these cells was performed by placing it gradually in an oven at 42 °C for 2 h, at 52 °C for overnight, and then at 62 °C for another overnight. Ultrathin sections (50–70 nm) of these blocks were cut using a Leica Ultramicrotome EM UC6. These ultrathin sections were collected from a 10% ethanol turf. The sections were contrasted using 1% aqueous uranyl acetate for 5 min and lead citrate in a CO_2-depleted atmosphere for 2–4 min. Hitachi H-8100 (75–200 kV) electron microscope (Japan) was used to evaluate the sections in 100 kV, and images were captured digitally using AMT V700 side mount camera.

2.15. Determination of glycolysis and mitochondrial respiration

Mitochondrial bioenergetics of DPSCs in the course of OB differentiation was measured at four different time points using an XF24 Extracellular Flux Analyzer (Seahorse Bioscience, Billerica, MA, USA). In brief, a sensor cartridge in Seahorse XF calibrant was hydrated at 37 °C in a non-CO_2 incubator for overnight. Pre-differentiated cells of various time points were dissociated and re-cultured uniformly at a density of 2×10^5 cells/well in a 24-well Seahorse cell culture plate for overnight. Seahorse plates were washed with Seahorse assay medium (Seahorse Bioscience) and filled with medium (500 μl) supplemented with pyruvate, glutamine, and glucose, and pH was adjusted to 7.4. Then plates were incubated in a non-CO_2 incubator at 37 °C for 1 h. Next, the oxygen consumption rate (OCR) and extracellular acidification rate (ECAR) of each well were measured by the XF24 Extracellular Flux Analyzer. For each time point, measurements were made from 4 independent inductions. For determination of oxidative phosphorylation properties, the ATP synthase inhibitor oligomycin (1.5 μM), un-coupler carbonyl cyanide-4- (trifluoromethoxy) phenylhydrazone (FCCP, 1 μM), complex III inhibitor rotenone, and antimycin A (0.5 μM) were added to the wells and sequentially measured using Seahorse Wave software 2.6.1. The OCR values determined the ATP turnover, maximal respiration, and reserve respiratory capacity. For determination of glycolytic properties, D-glucose (10 mM), oligomycin (1 μM), glycolytic inhibitor 2-deoxy-D-glucose (2-DG, 50 mM) were added accordingly. ECAR values were evaluated and calculated using the same software mentioned above.

2.16. Statistical analysis

All experiments were performed at least 3 times in a triplicate manner, and the results were displayed as mean ± SEM. Statistical analyses were performed using Graph Pad Prism 5.0 for Windows (Graph Pad Software, San Diego, CA, USA). Student's t-test was used to perform statistical analysis of RT-qPCR and Western blot graph results and p values less than 0.05 were considered significant (*).

3. Results

3.1. Effect of OB differentiation on the expression of KLF2 and autophagic genes

To determine molecular changes that occurred during OB differentiation in DPSCs, we induced OB differentiation using β-glycerophosphate and L-ascorbic acid (BGP + LAA), a traditional differentiation method, and evaluated expression levels of *KLF2* and various autophagy-related genes. We found that *KLF2* expression level was significantly increased, and genes, which are essential for autophagy vesicle formation (*BECN1, ATG5,* and *MAPLC3B*) were also significantly increased in a time-dependent manner during the course of differentiation (Fig. 1). Similarly, essential autophagy processing genes, *ATG3* and *ATG7,* were also upregulated during the course of

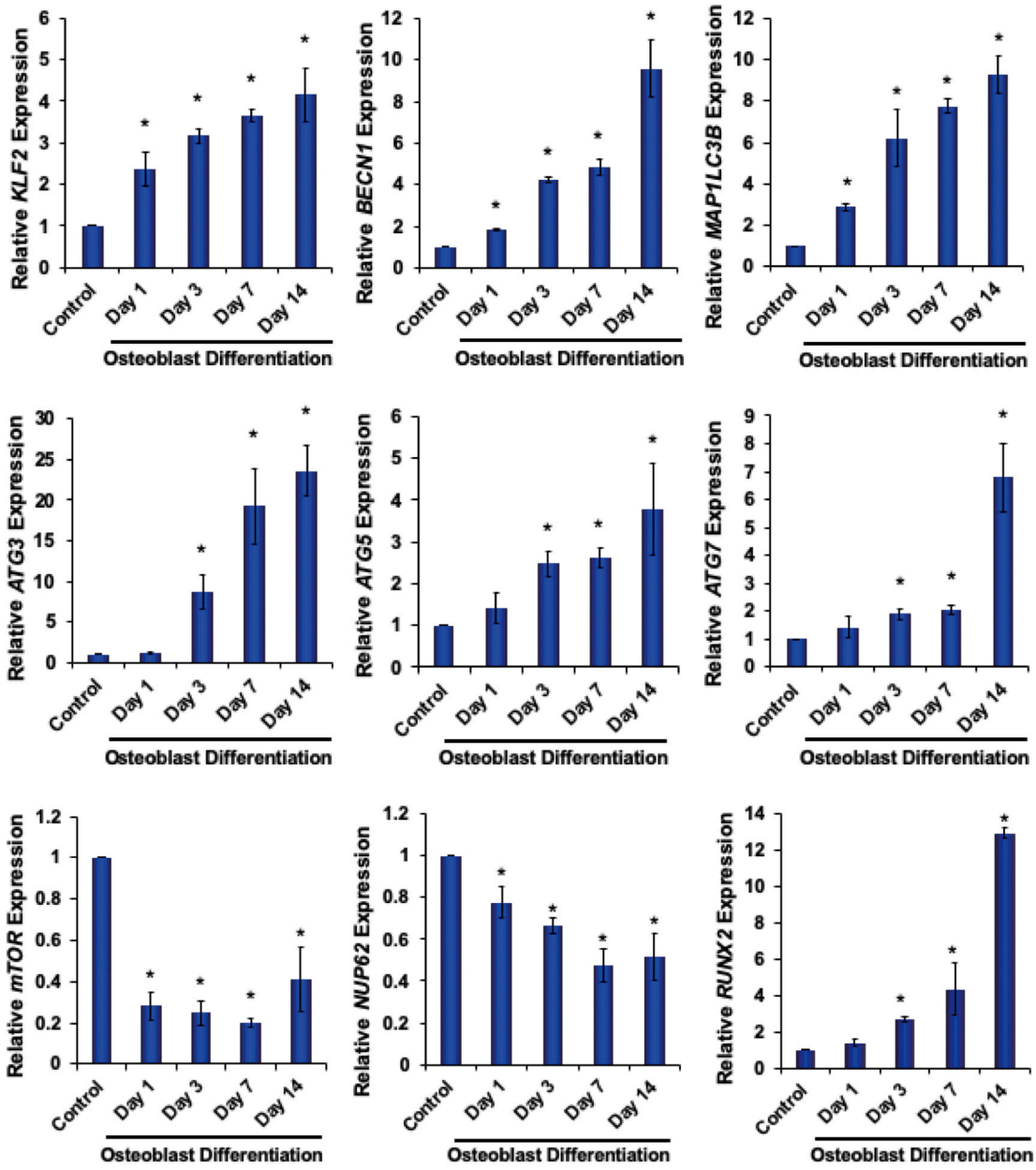

Fig. 1. ***OB differentiation induces expression of KLF2 and autophagic genes.*** DPSCs were induced to differentiate into OBs using β-glycerophosphate plus L-ascorbic acid (BGP + LAA), and cells were harvested at various time points, whereas, undifferentiated cells were considered as a control. Quantitative RT-PCR was performed with the isolated RNA for measuring expressions of *KLF2* and various autophagic genes during the course of differentiation. Star (*) indicates a statistical significance ($p < 0.05$) when compared to controls with differentiated cells (either of the days 1, 3, 7, or 14).

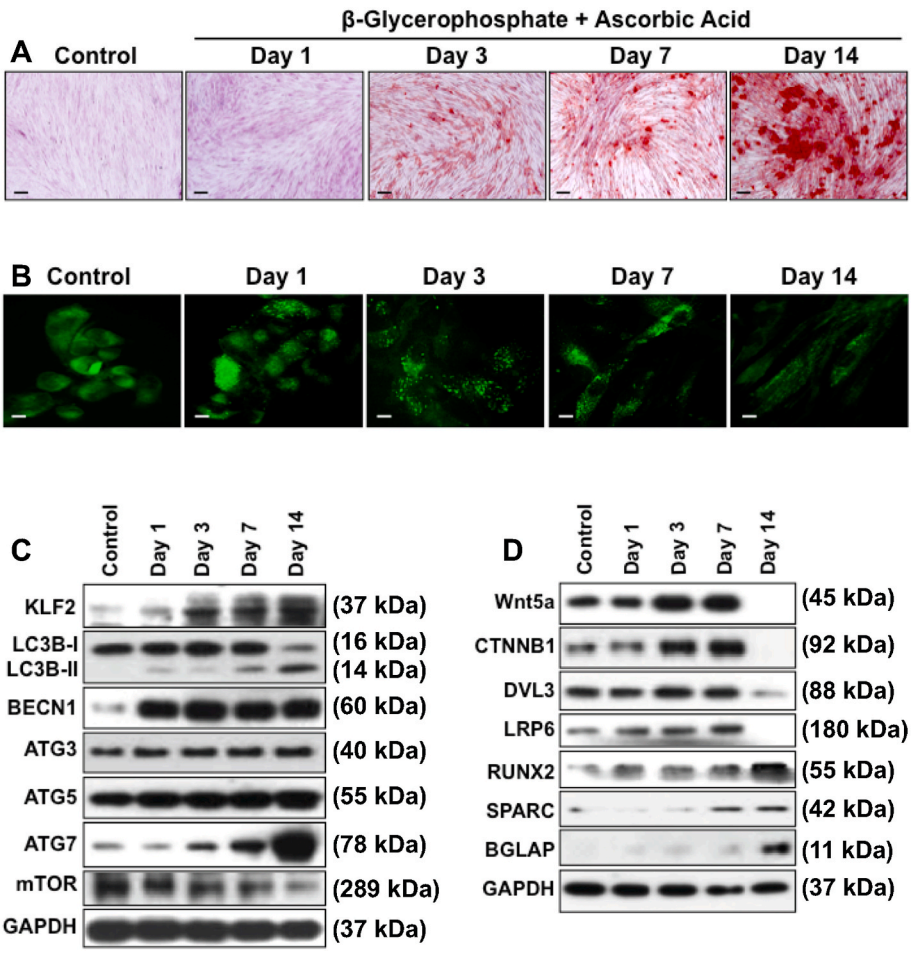

Fig. 2. ***OB differentiation induces KLF2 and autophagic proteins.*** DPSCs were induced to differentiate into OBs using BGP + LAA, and cells were either stained or harvested at various time points, and undifferentiated cells were considered as a control. **A.** Alizarin red staining of the differentiated cells for the detection of OB differentiation. **B.** MDC staining of the differentiated cells for the detection of autophagic vesicles. **C and D.** Western blot images of the isolated proteins during the course of differentiation (1, 3, 7, and 14 days). (For interpretation of the references to colour in this figure legend, the reader is referred to the Web version of this article.)

differentiation. We further found that mRNA expression of the negative regulator of autophagy, mTOR was significantly decreased after induction of differentiation. Finally, we also observed that *Runx2* the essential transcription factor for OB differentiation was upregulated nearly 13-fold after 14 days of differentiation (Fig. 1). These data provide evidence that OB differentiation in DPSC induced a transcriptional regulator, *KLF2*, along with autophagy-associated genes.

3.2. Effect of OB differentiation on KLF2 and autophagic molecules

To assess whether gene expressions were translated into proteins, we next induced OB differentiation in DPSCs and confirmed with Alizarin Red staining, which showed prominent mineralization at later time points (Fig. 2A). Next, we verified autophagic vesicles formation during the course of OB differentiation using monodansylcadaverine (MDC) staining and found that autophagic vesicles were prominent as differentiation progresses (Fig. 2B). This MDC staining confirms that an increased number of autophagosomes were recruited in the cytoplasm of DPSC during OB differentiation. To determine the association between induction of KLF2 and upregulation of autophagy with OB differentiation, we performed western blotting from isolated proteins during the course of OB differentiation. We demonstrate a novel finding that our protein of interest KLF2 was increased during OB differentiation. In addition, we found that the levels of autophagic proteins such as BECN1, ATG3, ATG5, ATG7, and cleaved LC3B-II were increased, and concomitantly decreased the level of mTOR during the course of OB differentiation (Fig. 2C and Fig. S2A). Next, we investigated some of the Wnt signaling pathway molecules that are associated with OB differentiation, and some osteoblast marker proteins like osteocalcin (BGLAP), osteonectin (SPARC); and found that those above-mentioned molecules were increased during the course of OB differentiation (Fig. 2D and Fig. S2B).

3.3. Effect of KLF2 modulation on autophagy and it's regulating molecules

To investigate the correlative effect on autophagy and it's regulating molecules with modulation of *KLF2,* we knocked down or overexpressed *KLF2* in DPSCs, which were cultured in a complete medium using si*KLF2* and Ad*KLF2* constructs respectively. MDC staining revealed that the knockdown of *KLF2* resulted in a decreased number of autophagosomes, and overexpression of *KLF2* resulted in an increased number of autophagosomes, respectively (Fig. 3A and C). Western blot analysis revealed that partial knockdown of *KLF2* resulted in decreased levels of autophagy regulating molecules, such as LC3B-II:LC3B-I ratio, BECN1, ATG3, ATG5, and ATG7 (Fig. 3B and Fig. S3A). On the other hand, after overexpression of *KLF2,* all tested autophagic molecules (LC3B-II:LC3B-I ratio, BECN1, ATG5, and ATG7) were markedly increased (Fig. 3D and Fig. S3B). These results indicate that the involvement of *KLF2* in the autophagic process in DPSCs.

3.4. Effect of KLF2 or ATG7 or BECN1 knockdown on autophagy and OB markers during OB differentiation

We next sought to determine the consequences of *KLF2* knockdown during OB differentiation of DPSCs culturing with BGP + LAA containing medium for 72 h. More than 70% knockdown of *KLF2* was achieved. Partial knockdown of *KLF2* resulted in decreased levels of autophagic

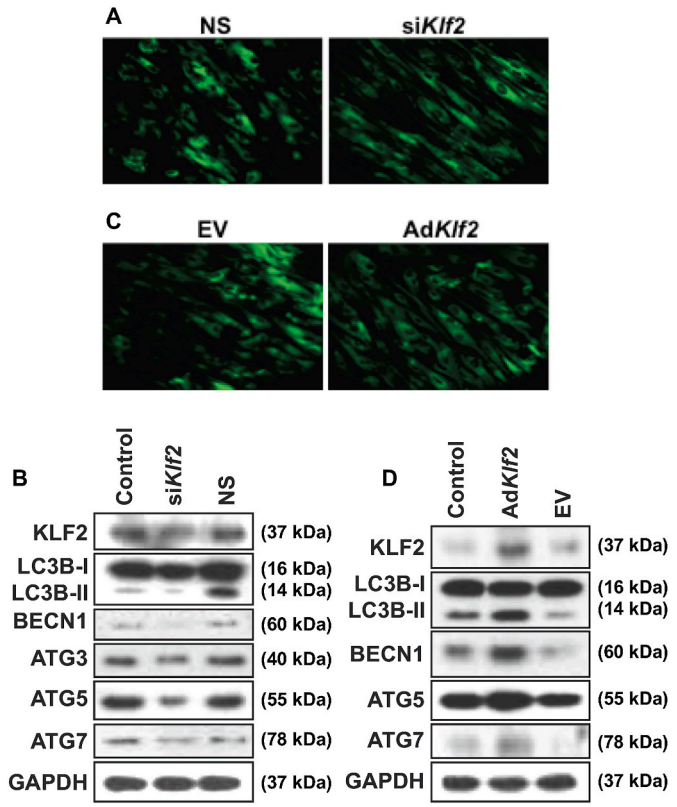

Fig. 3. *KLF2* modulation positively affects autophagic vesicle formation and autophagy-related molecules. *KLF2* was knocked down or overexpressed in DPSCs and evaluated for the formation of autophagic vesicles and autophagy-related molecules. **A and C.** MDC staining's after knockdown and over-expression of *KLF2*. **B and D.** Western blot images of the KLF2 and autophagy-related proteins after knockdown and overexpression of *KLF2*.

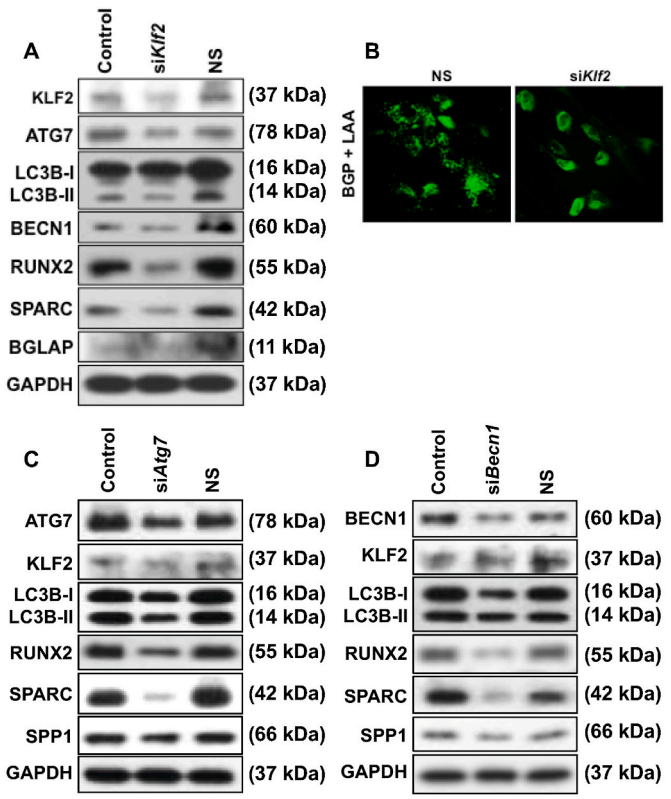

Fig. 4. Knockdown of *KLF2* or *ATG7* or *BECN1* reduced autophagy-related molecules and OB differentiation-related markers. *KLF2* or *ATG7* or *BECN1* was knocked down in DPSCs and cells were cultured in β-glycerophosphate plus L-ascorbic acid-containing medium. **A.** Western blot analysis for detection of autophagy-related molecules and OB differentiation-related markers after knockdown of *KLF2*. **B.** MDC staining for detection of autophagy vesicles after knockdown of *KLF2*. **C.** Western blot analysis for detection of autophagy-related molecules and OB differentiation-related markers after knockdown of *ATG7*. **D.** Western blot analysis for detection of autophagy-related molecules and OB differentiation-related markers after knockdown of *BECN1*.

proteins (ATG7, LC3BII:LC3BI ratio, BECN1) as well as OB differentiation-related marker proteins, such as RUNX2, SPARC, and BGLAP (Fig. 4A and Fig. S4A). These findings confirmed that *KLF2* positively correlates with autophagic molecules and OB differentiation-related molecules. MDC staining further confirmed the decreased amount of autophagic vesicles in DPSCs cultured in OB differentiation medium after knockdown of *KLF2* (Fig. 4B).

After confirming a positive correlation with *KLF2* and autophagy-related molecules, we next wanted to determine whether autophagy-related molecules also have the reciprocal effect on *KLF2*, by knocking down of two of the important autophagy-related molecules *ATG7* and *BECN1* in DPSCs. Partial knockdown of *ATG7* resulted in a strikingly decreased level of KLF2 and concomitantly reduced levels of autophagy-related molecules LC3BII:LC3BI ratio, as well as OB differentiation-related marker proteins like RUNX2, SPARC, and SPP1 (osteopontin) (Fig. 4C and Fig. S4B). Similarly, partial knockdown of *BECN1* also resulted in a reduced level of KLF2, and concomitantly reduced levels of autophagy-related molecules LC3BII:LC3BI ratio, as well as OB differentiation-related marker proteins, includes RUNX2, SPARC, and SPP1 (Fig. 4D and Fig. S4C). Together, these results confirm that *KLF2* and autophagy-related molecules along with OB differentiation-related molecules are in positive correlation.

3.5. Effect of induced autophagy on KLF2

We next verified the effect of known inducers of autophagy, such as starvation and addition of rapamycin (mTOR inhibitor) on DPSCs during the culture. After starvation, we found that a strikingly increased level of KLF2 protein in DPSCs along with expected higher levels of autophagic proteins (LC3BII:LC3BI ratio, ATG5, ATG7, BECN1) and concomitant decreased level of mTOR protein (Fig. 5A and Fig. S5A).

After addition of rapamycin (50, 150 and 300 nM) doses to the culture, we also found that the remarkably increased level of KLF2 in DPSCs along with higher levels of autophagic proteins (LC3BII:LC3BI ratio, ATG5, ATG7, and BECN1) and concomitantly decreased level of mTOR protein (Fig. 5B and Fig. S5B). MDC staining further confirmed that the formation of autophagic vesicles in DPSCs after starvation, and addition of rapamycin (Fig. 5C). These results further confirmed that KLF2 has an important role during autophagy induction.

3.6. Effect of OB differentiation on mitochondria in DPSCs

To detect the involvement of mitochondria, cellular staining was performed after OB differentiation of DPSCs. Mitochondrial membrane potential (MMP) was determined using JC1 dye. Staining revealed that MMP was decreased after OB differentiation, which is a hallmark of mitophagy. We observed that a higher number of aggregates in undifferentiated cells (Fig. 6A, upper panels), and the number of aggregates was decreased upon induction of OB differentiation (Fig. 6A, lower panels).

We next performed Western blot analysis for PINK1 and Parkin proteins accumulation during OB differentiation in DPSCs. Western blot analysis revealed that both PINK1 and parkin protein levels were much higher in differentiated cells compared to undifferentiated DPSCs (Fig. 6B and Fig. S6).

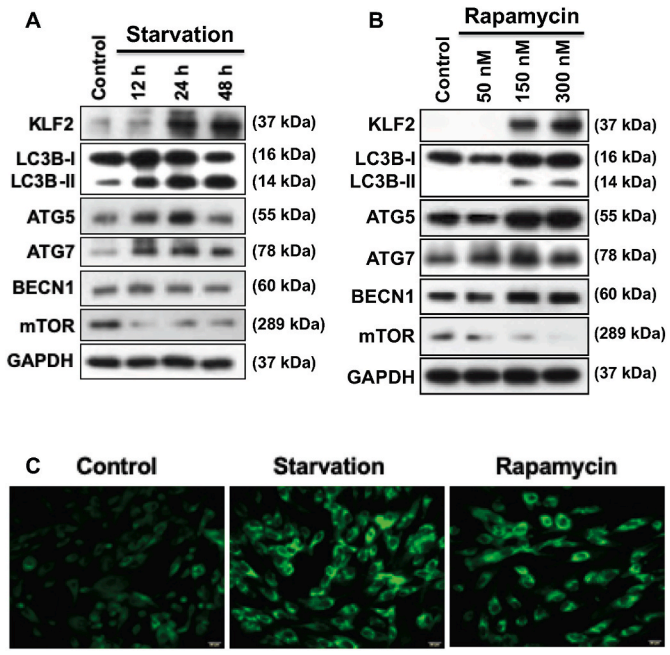

Fig. 5. Starvation or addition of rapamycin to DPSCs induced autophagy and KLF2 levels. A. Western blot images of the level of KLF2 and autophagy-related molecules in DPSCs after starvation at various time points. **B.** Western blot images of the level of KLF2 and autophagy-related molecules in DPSCs after the addition of various doses of rapamycin. **C.** MDC staining for detection of autophagy vesicles after serum starvation (for 24 h) and addition of rapamycin (300 nM).

To confirm mitophagy, ultrastructural visualization was performed by using the bio transmission electron microscopy method (BioTEM) in DPSCs after OB differentiation and undifferentiated cells were kept as a control. Depicted images revealed that the presence of healthy mitochondria and the absence of double-layered vacuoles in control cells (Fig. 6C, left panels). However, many autophagic vacuoles, damaged mitochondria, and engulfed mitochondria were observed in OB differentiated cells (Fig. 6C, right panels). These results indicate that the involvement of mitophagy during the OB differentiation in DPSCs.

To investigate the status of intracellular functions during the OB differentiation, we assessed the level of reactive oxygen species (ROS) generation, mitochondrial superoxide production, and intracellular Ca^{2+} production after the OB differentiation. We found that a significantly decreased amount of ROS and mitochondrial superoxide production after OB differentiation in DPSCs compared to the undifferentiated control cells (Fig. 6D upper and lower panels respectively). However, the level of intracellular calcium was significantly increased after OB differentiation compared to controls (Fig. 6D, middle panel).

3.7. Effect on oxygen consumption rate and extracellular acidification rate during the OB differentiation in DPSC

For measuring glycolysis and oxidative phosphorylation (through oxygen consumption) simultaneously in live cells Seahorse extracellular flux analysis was performed. Data revealed that OB differentiation decreased the oxygen consumption rate (OCR), which is reflected as mitochondrial respiration at basal, maximal respiration, spare respiratory capacity conditions, and reduced the level of ATP production after OB differentiation in all-time points tested (1, 3, 7, and 14 days; Fig. 7A and Fig. S7A).

In addition, we also performed a glycolytic stress analysis using a mito-stress flux analyzer. Glycolytic ATP synthesis is compulsorily dependent on glycolytic carbon flux, glycolytic capacity is therefore measured for the maximum capacity of glycolysis to generate ATP. We found that increased levels of extracellular acidification rate (ECAR) in the non-glycolytic acidification, and glycolytic capacity condition after OB differentiation (Fig. 7B and Fig. S7B). These findings confirm that mitochondrial metabolic functions were also affected during OB differentiation of DPSCs.

3.8. Epigenetic regulation of ATG7 promoter after induction of osteoblastic differentiation

After establishing *ATG7* expression is directly correlated with *KLF2* expression, we further investigated the epigenetic regulatory mechanisms of the *ATG7* gene during OB differentiation. From the UCSC genome browser, we found that enrichment sites for epigenetic marks are located at +0.5 kb (upstream) of the human *ATG7* transcriptional start site (TSS). We examined whether *KLF2* is involved in regulating *ATG7* expression through binding to its promoter region, we performed *KLF2*-chromatin immunoprecipitation (ChIP) analysis in OB differentiated cells keeping undifferentiated cells as a control using two different primer sequences from two different regions of the promoter (Fig. 8A and B). In both cases, in control cells, *KLF2* binding was detected in the promoter region of *ATG7*. However, *KLF2* binding was significantly increased in OB-differentiated cells determined by evaluating the levels of H3K4me3 and H3K27Ac marks (Fig. 8). Taken together these data confirm that KLF2 expression was not only increased in differentiated osteoblast cells but also binding efficiency of KLF2 was increased on *ATG7* promoter, which resulted in activation of *ATG7* gene through the enrichment of methylation of H3K4 and acetylation of H3K27 molecules. Taken together these data support that increased level of KLF2 binding resulted in increased levels of H3K4me3 and H3K27Ac during osteoblastic differentiation.

4. Discussion

Osteoblast differentiation has a significant impact on the regulation of bone homeostasis, and dysregulation in this process causes various cartilage and bone-related pathologies. However, mechanisms of OB differentiation from precursor MSCs remain elusive. On the other hand, autophagy is critical in maintaining mesenchymal stemness and differentiation [38], cellular energy generation, and recycling of metabolic precursors, which are required for cell survival. Autophagy and KLF2 share common activation and regulatory pathways in the maintenance of endothelial phenotype and survival [39]. For instance, the lipid-lowering drug, statin induces KLF2 along with autophagy in prostate cancer cells [40]. In addition, a conserved KLF-autophagy pathway modulates nematode lifespan and mammalian age-associated vascular dysfunction [41]. These findings provide a link between autophagy and KLF2. We recently showed that KLF2 negatively regulates autophagy during osteoclast differentiation [11]. The current study focused on revealing the KLF2-mediated molecular regulation of the autophagic pathway during OB differentiation of DPSC, which will provide a new insight into development and treatment options for bone-related diseases.

Induction of autophagy is essential for OB cell development and mineralization [12]. With our initial findings, we observed that autophagy was increased during OB differentiation, which was confirmed by the elevated levels of autophagic markers, such as, LC3B-II, BECN1, ATG3, ATG5, and ATG7 (Figs. 1 and 2). To investigate the direct role of KLF2 on OB differentiation, we performed *KLF2* loss-of-function experiments, which showed a positive correlation in reducing both autophagy (LC3B-II, BECN1, and ATG7), and OB differentiation (RUNX2, BGLAP, and SPARC) specific markers (Fig. 3). In concordance with our findings, recent evidence showed that KLF2 was upregulated during OB differentiation of mouse pre-osteoblastic cells, and KLF2 enhanced transcriptional activity of the Runx2 [42]. Next, we investigated the effect of autophagy on *KLF2* expression. Two different autophagic gene-specific

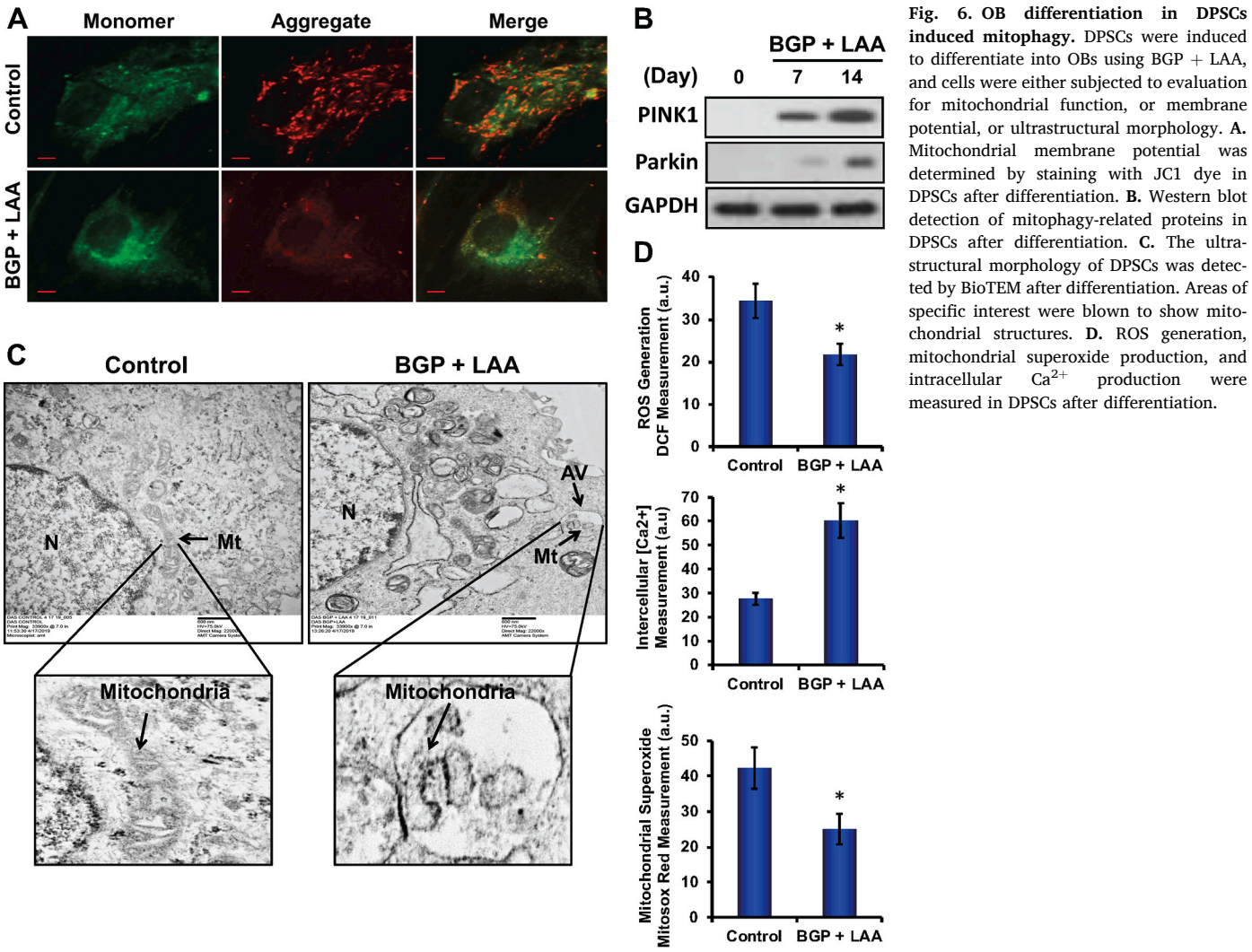

Fig. 6. OB differentiation in DPSCs induced mitophagy. DPSCs were induced to differentiate into OBs using BGP + LAA, and cells were either subjected to evaluation for mitochondrial function, or membrane potential, or ultrastructural morphology. **A.** Mitochondrial membrane potential was determined by staining with JC1 dye in DPSCs after differentiation. **B.** Western blot detection of mitophagy-related proteins in DPSCs after differentiation. **C.** The ultrastructural morphology of DPSCs was detected by BioTEM after differentiation. Areas of specific interest were blown to show mitochondrial structures. **D.** ROS generation, mitochondrial superoxide production, and intracellular Ca^{2+} production were measured in DPSCs after differentiation.

siRNAs (si*ATG7* and si*BECN1*) were employed, showing inhibition of autophagy, and reducing expression of KLF2 (Fig. 4). This observation indicated a direct or indirect role of autophagy-mediated KLF2 regulation during OB differentiation of DPSCs.

The involvement of WNT5A in OB differentiation from MSCs [43] and bone formation was reported [44]. Next investigated the effect of OB differentiation of DPSCs on Wnt signaling molecules. Increased levels of WNT5A, CTNNB1 (β-Catenin), DVL3, and LRP6 were observed during OB differentiation (up to 7 days), confirming the involvement of the Wnt pathway. These findings support our previous data showing ferutinin directs OB differentiation of DPSCs through the Wnt signaling pathway [4], and involvement of Wnt signaling-induced Warburg effect, which is an activator of OB differentiation [45]. This data also indicates possible crosstalk among autophagy, KLF2, and Wnt signaling during OB differentiation. Conversely, we observed that after the addition of rapamycin (mTOR inhibitor) or starvation facilitated upregulation of autophagy, resulted in the upregulation of KLF2 (Fig. 5) further confirming a positive correlation between autophagy and KLF2 in DPSCs.

Calcium (Ca^{2+}) plays a crucial role in bone formation. Moreover, OBs not only play a central role in regulating skeletal structure but also in maintaining calcium homeostasis [46]. We observed an upregulation of intracellular calcium level during OB differentiation (Fig. 6), which is aligned with the previous finding showing the elevated level of intercellular calcium during OB differentiation [47]. Mitochondrial damage via excess ROS, mitochondrial superoxide, and protein oxidation, can inhibit OB differentiation [48]. We found that a reduced level of ROS and mitochondrial superoxide production during OB differentiation, which established that DPSCs maintain healthy mitochondrial status by reducing the ROS level. Next wanted to find how the ROS level was reduced and its' possible defense mechanism during OB differentiation. It was reported that mitophagy helps to clear defective mitochondrion and reduces ROS level in growing cells under mild stress conditions, thus assuring cell survival. Moreover, ROS initiates signaling mechanisms of autophagy [49]. Additionally, our data revealed, a decreased level of mitochondrial membrane potential during OB differentiation (Fig. 6). Decreased mitochondrial membrane potential may lead to lower ATP generation, causing arrested differentiation or becoming abnormal due to insufficient supply of energy. To meet the higher demand for energy during differentiation, mitochondria produce higher ROS, and that damages itself [48], and damaged mitochondria enter into mitochondrial fission procedure [50]. This could induce both autophagy and mitochondria-selective mitophagy, which can be detected with an elevated level of PINK1 and then parkin expressions [51]. To confirm this phenomenon, we analyzed PINK1 and Parkin expressions during OB differentiation. Observations confirmed the increased levels of PINK1 and Parkin accumulations in OB differentiated cells (Fig. 6). Further, the analysis of mitochondrial structure through BioTEM confirmed the presence of mitophagy during OB differentiation (Fig. 6). Together our findings established the cell defense mechanism via autophagy and mitophagy during OB differentiation in DPSC. Moreover, autophagy and

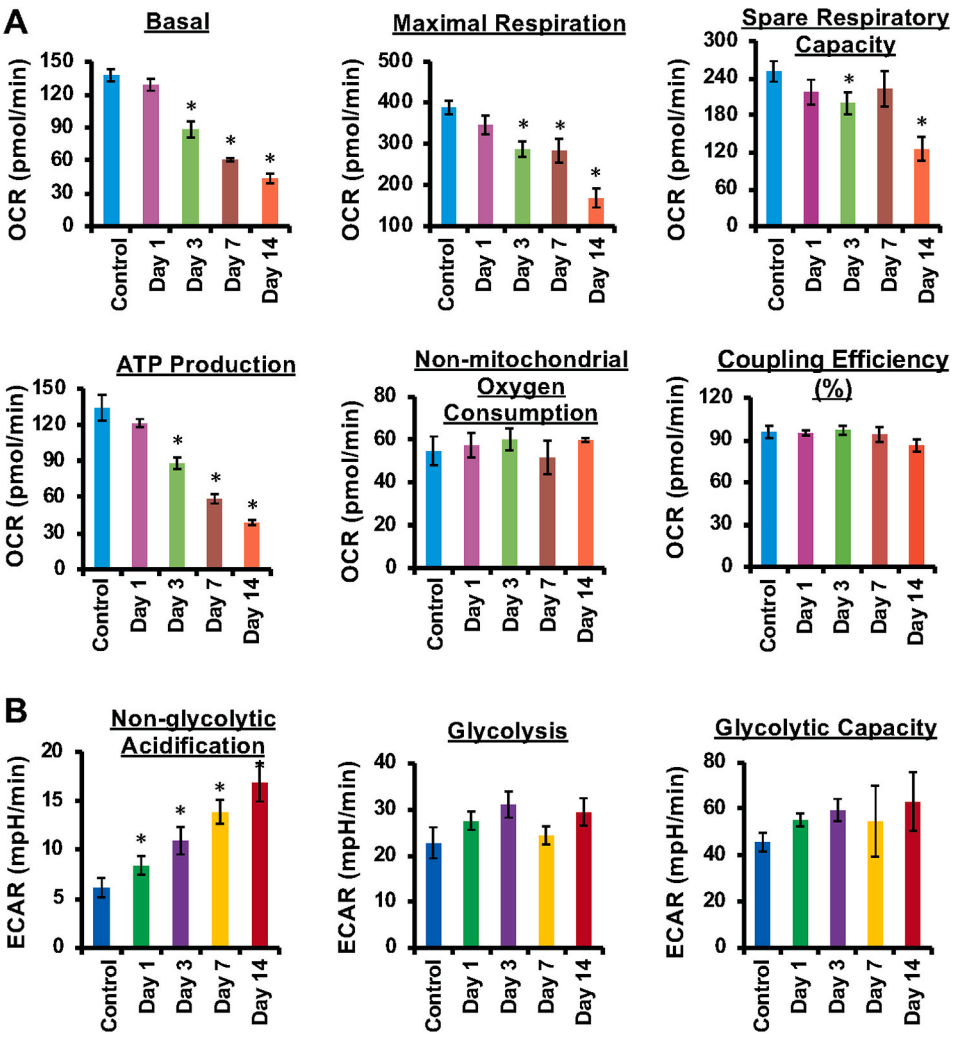

Fig. 7. Reduced oxygen consumption rate and increased extracellular acidification rate during OB differentiation. A. Seahorse extracellular flux analysis revealed that a decreased level of oxygen consumption rate (OCR), which is an indicator of mitochondrial respiration at basal, maximal respiration, spare respiratory capacity conditions, and reduced the level of ATP production during OB differentiation. **B.** In addition, flux analysis also revealed that an increased level of extracellular acidification rate (ECAR) in the non-glycolytic acidification, and the glycolytic capacity conditions during OB differentiation.

mitophagy mediated removal of cytosolic damaged proteins or organelles provide cells with amino acids that are oxidized and supporting ATP production [52].

Mitochondrial metabolism plays a vital role in cellular functioning, and the controlled regulation of glycolysis and oxidative phosphorylation fluxes is crucial for self-renewal and differentiation of stem cells [53]. The number and function of mitochondria in cells varies with the differential energy demands [54]. Enhancement of glycolysis improves reprogramming efficiency of human primary somatic cells [55]. We found that a decreased mitochondrial metabolism and simultaneously increased glycolytic metabolism including glycolytic reserve capacity in OB differentiated cells (Fig. 7). This is in accordance with studies showing aerobic glycolysis, also known as the Warburg effect, where increased levels of key glycolytic enzymes were found during OB differentiation [45]. In addition, reduced ATP demand and mitochondrial activity in neural differentiation from human embryonic stem cells [56], a switch from mitochondrial oxidative phosphorylation to glycolysis during reprogramming of iPSC [57], which were in support of our findings.

Recently, the role of epigenetic mechanisms, such as DNA methylation and histone modifications in regulating autophagy has been highlighted. *KLF2* is a zinc finger transcription factor involved in early differentiation of cells [58]. To define the *KLF2*-mediated direct regulation of the autophagic pathway in OB differentiated cells, we examined the *KLF2* binding profiles around TSS of *ATG7* promoter. There are two well-studied histone marks associated with active promoters and enhancers, H3-trimethyl-Lys4 (H3K4me3) and H3-acetyl-Lys27 (H3K27Ac), which initiate elongation by making the chromatin accessible to RNA polymerase II [59,60]. We have designed primers to analyze *KLF2* binding along with H3K4me3 and H3K27Ac around the TSS region of *ATG7* in OB differentiated DPSCs. ChIP analysis revealed that OB differentiation was associated with an increased level of *KLF2* binding along with H3K4me3 and H3K27 expressions on around the TSS region of *ATG7* (Fig. 8). Taken together our data established that the KLF2-autophagy pathway positively regulates OB differentiation in DPSCs.

5. Conclusion

In sum, herein, we provide the first evidence of the induction of KLF2 during the OB differentiation of DPSCs, which is corroborated with autophagy-related molecules. We have confirmed the involvement of KLF2 and autophagy using both loss-of-function and gain-of-function approaches for both the *KLF2* gene and two autophagic genes, such as *ATG7* and *BECN1*. In addition, we showed that mitophagy along with their metabolic functions is involved in this process. We further confirmed with epigenetic studies showing that KLF2 is important in regulating autophagy. These results provide evidence that the autophagy process is important during OB differentiation, and *KLF2* critically regulates autophagy/mitophagy. These results suggest that a strategy on targeting KLF2 in modulating autophagy, more precisely mitophagy, could be used to develop a new potential regenerative

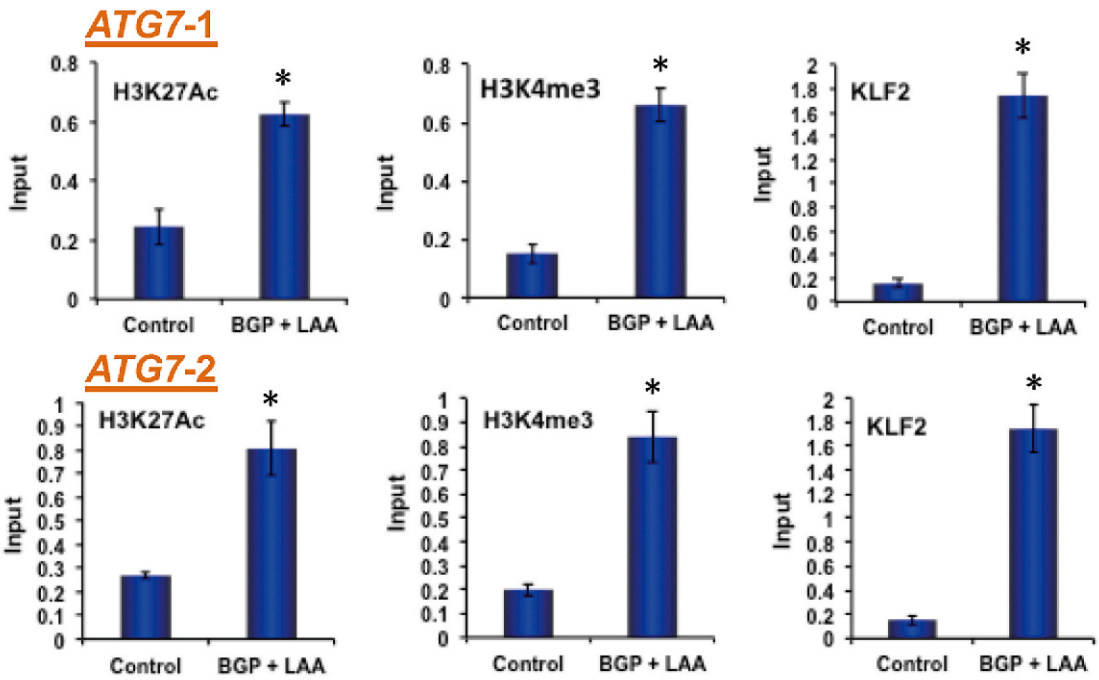

Fig. 8. ***KLF2*** **regulates the** ***ATG7*** **gene epigenetically during OB differentiation**. Autophagy signaling pathway molecule *ATG7* was analyzed using KLF2-ChIP and quantitative PCR methods after the differentiation of DPSCs. Active marks of the *ATG7* gene for both H3K4me3 and H3K27Ac molecules were evaluated in the promoter site using two different primers such as **A.** ATG7-1 and **B.** ATG7-2, and shown graphically. Star (*) indicates a statistical significance ($p < 0.05$) when compared to controls with differentiated cells.

therapeutic approach for bone disorders, such as arthritis and osteoporosis.

Funding

This work was supported in part by National Institutes of Health grants, R01AR068279 (NIAMS), STTR 1R41EY024217 (NEI), and STTR 1R41AG057242 (NIA). The funders had no role in study design, data collection, and analysis, decision to publish, or preparation of the manuscript.

Author contributions

All authors were involved in drafting the article or revising it critically for important intellectual content, and all authors approved the final version to be published. Study conception, design, and manuscript writing: JM and HD. Acquisition of data: JM, MD, CG, and HD. Analysis and interpretation of data: JM and HD.

Declaration of competing interest

Authors do not have any potential conflict of interest to disclose.

Appendix A. Supplementary data

Supplementary data to this article can be found online at https://doi.org/10.1016/j.redox.2020.101622.

References

[1] M.F. Pittenger, A.M. Mackay, S.C. Beck, R.K. Jaiswal, R. Douglas, J.D. Mosca, M. A. Moorman, D.W. Simonetti, S. Craig, D.R. Marshak, Multilineage potential of adult human mesenchymal stem cells, Science 284 (5411) (1999) 143–147.
[2] H.B. Zhao, Membrane trafficking in osteoblasts and osteoclasts: new avenues for understanding and treating skeletal diseases, Traffic 13 (10) (2012) 1307–1314.
[3] C. Nombela-Arrieta, J. Ritz, L.E. Silberstein, The elusive nature and function of mesenchymal stem cells, Nat. Rev. Mol. Cell Biol. 12 (2) (2011) 126–131.
[4] D.N. Rolph, M. Deb, S. Kanji, C.J. Greene, M. Das, M. Joseph, R. Aggarwal, B. Leblebicioglu, H. Das, Ferutinin directs dental pulp-derived stem cells towards the osteogenic lineage by epigenetically regulating canonical Wnt signaling, Biochim. Biophys. Acta (BBA) - Mol. Basis Dis. 1866 (4) (2020) 165314, https://doi.org/10.1016/j.bbadis.2018.10.032. Epub 2018 Nov 6.
[5] D.J. Klionsky, S.D. Emr, Autophagy as a regulated pathway of cellular degradation, Science 290 (5497) (2000) 1717–1721.
[6] D.C. Rubinsztein, G. Marino, G. Kroemer, Autophagy Aging,Cell 146 (5) (2011) 682–695.
[7] N. Mizushima, B. Levine, A.M. Cuervo, D.J. Klionsky, Autophagy fights disease through cellular self-digestion, Nature 451 (7182) (2008) 1069–1075.
[8] J. Maity, B. Das, V.A. Bohr, P. Karmakar, Acidic domain of WRNp is critical for autophagy and up-regulates age associated proteins, DNA Repair 68 (2018) 1–11.
[9] Y. Choi, J.W. Bowman, J.U. Jung, Autophagy during viral infection - a double-edged sword, Nat. Rev. Microbiol. 16 (6) (2018) 341–354.
[10] N. Mizushima, Autophagy: process and function, Genes Dev. 21 (22) (2007) 2861–2873.
[11] D. Laha, M. Deb, H. Das, KLF2 (kruppel-like factor 2 [lung]) regulates osteoclastogenesis by modulating autophagy, Autophagy 15 (12) (2019) 2063–2075.
[12] M. Nollet, S. Santucci-Darmanin, V. Breuil, R. Al-Sahlanee, C. Cros, M. Topi, D. Momier, M. Samson, S. Pagnotta, L. Cailleteau, S. Battaglia, D. Farlay, R. Dacquin, N. Barois, P. Jurdic, G. Boivin, D. Heymann, F. Lafont, S.S. Lu, D. W. Dempster, G.F. Carle, V. Pierrefite-Carle, Autophagy in osteoblasts is involved in mineralization and bone homeostasis, Autophagy 10 (11) (2014) 1965–1977.
[13] G.M. Cereghetti, L. Scorrano, The many shapes of mitochondrial death, Oncogene 25 (34) (2006) 4717–4724.
[14] A.B. Harbauer, R.P. Zahedi, A. Sickmann, N. Pfanner, C. Meisinger, The protein import machinery of mitochondria-a regulatory hub in metabolism, stress, and disease, Cell Metabol. 19 (3) (2014) 357–372.
[15] P.M. Quiros, T. Langer, C. Lopez-Otin, New roles for mitochondrial proteases in health, ageing and disease, Nat. Rev. Mol. Cell Biol. 16 (6) (2015) 345–359.
[16] D.C. Chan, Fusion and fission: interlinked processes critical for mitochondrial health, Annu. Rev. Genet. 46 (2012) 265–287.
[17] H. Aguilaniu, L. Gustafsson, M. Rigoulet, T. Nystrom, Asymmetric inheritance of oxidatively damaged proteins during cytokinesis, Science 299 (5613) (2003) 1751–1753.
[18] P. Katajisto, J. Dohla, C.L. Chaffer, N. Pentinmikko, N. Marjanovic, S. Iqbal, R. Zoncu, W. Chen, R.A. Weinberg, D.M. Sabatini, Stem cells. Asymmetric apportioning of aged mitochondria between daughter cells is required for stemness, Science 348 (6232) (2015) 340–343.
[19] A.M. Pickrell, R.J. Youle, The roles of PINK1, parkin, and mitochondrial fidelity in Parkinson's disease, Neuron 85 (2) (2015) 257–273.
[20] J. Nunnari, A. Suomalainen, Mitochondria: in sickness and in health, Cell 148 (6) (2012) 1145–1159.
[21] M.P. Murphy, How mitochondria produce reactive oxygen species, Biochem. J. 417 (1) (2009) 1–13.

[22] L.A. Sena, N.S. Chandel, Physiological roles of mitochondrial reactive oxygen species, Mol. Cell 48 (2) (2012) 158–167.
[23] J. Yun, T. Finkel, Mitohormesis Cell Metab. 19 (5) (2014) 757–766.
[24] H. Murata, H. Takamatsu, S. Liu, K. Kataoka, N.H. Huh, M. Sakaguchi, NRF2 regulates PINK1 expression under oxidative stress conditions, PLoS One 10 (11) (2015), e0142438.
[25] M. Frank, S. Duvezin-Caubet, S. Koob, A. Occhipinti, R. Jagasia, A. Petcherski, M. O. Ruonala, M. Priault, B. Salin, A.S. Reichert, Mitophagy is triggered by mild oxidative stress in a mitochondrial fission dependent manner, Biochim. Biophys. Acta 1823 (12) (2012) 2297–2310.
[26] B.B. McConnell, V.W. Yang, Mammalian Kruppel-like factors in health and diseases, Physiol. Rev. 90 (4) (2010) 1337–1381.
[27] M.A. Wani, S.E. Wert, J.B. Lingrel, Lung Kruppel-like factor, a zinc finger transcription factor, is essential for normal lung development, J. Biol. Chem. 274 (30) (1999) 21180–21185.
[28] C.M. Carlson, B.T. Endrizzi, J. Wu, X. Ding, M.A. Weinreich, E.R. Walsh, M. A. Wani, J.B. Lingrel, K.A. Hogquist, S.C. Jameson, Kruppel-like factor 2 regulates thymocyte and T-cell migration, Nature 442 (7100) (2006) 299–302.
[29] C.J. Pang, W. Lemsaddek, Y.N. Alhashem, C. Bondzi, L.C. Redmond, N. Ah-Son, C. I. Dumur, K.J. Archer, J.L. Haar, J.A. Lloyd, M. Trudel, Kruppel-like factor 1 (KLF1), KLF2, and Myc control a regulatory network essential for embryonic erythropoiesis, Mol. Cell Biol. 32 (13) (2012) 2628–2644.
[30] P. Sangwung, G.J. Zhou, L. Nayak, E.R. Chan, S. Kumar, D.W. Kang, R.L. Zhang, X. D. Liao, Y. Lu, K. Sugi, H. Fujioka, H. Shi, S.D. Lapping, C.C. Ghosh, S.J. Higgins, S. M. Parikh, H. Jo, M.K. Jain, KLF2 and KLF4 control endothelial identity and vascular integrity, Jci Insight 2 (4) (2017).
[31] H. Das, A. Kumar, Z. Lin, W.D. Patino, P.M. Hwang, M.W. Feinberg, P. K. Majumder, M.K. Jain, Kruppel-like factor 2 (KLF2) regulates proinflammatory activation of monocytes, Proc. Natl. Acad. Sci. U. S. A. 103 (17) (2006) 6653–6658.
[32] M. Das, J. Lu, M. Joseph, R. Aggarwal, S. Kanji, B.K. McMichael, B.S. Lee, S. Agarwal, A. Ray-Chaudhury, O.H. Iwenofu, P. Kuppusamy, V.J. Pompili, M. K. Jain, H. Das, Kruppel-like factor 2 (KLF2) regulates monocyte differentiation and functions in mBSA and IL-1beta-induced arthritis, Curr. Mol. Med. 12 (2) (2012) 113–125.
[33] M. Das, D. Laha, S. Kanji, M. Joseph, R. Aggarwal, O.H. Iwenofu, V.J. Pompili, M. K. Jain, H. Das, Induction of Kruppel-like factor 2 reduces K/BxN serum-induced arthritis, J. Cell Mol. Med. 23 (2) (2019) 1386–1395.
[34] M. Das, M. Deb, D. Laha, M. Joseph, S. Kanji, R. Aggarwal, O.H. Iwenofu, V. J. Pompili, W. Jarjour, H. Das, Myeloid kruppel-like factor 2 critically regulates K/BxN serum-induced arthritis, Cells 8 (8) (2019).
[35] J.C. Yeo, J. Jiang, Z.Y. Tan, G.R. Yim, J.H. Ng, J. Goke, P. Kraus, H. Liang, K. A. Gonzales, H.C. Chong, C.P. Tan, Y.S. Lim, N.S. Tan, T. Lufkin, H.H. Ng, Klf2 is an essential factor that sustains ground state pluripotency, Cell Stem Cell 14 (6) (2014) 864–872.
[36] H.R. Chu, Y.C. Sun, Y. Gao, X.M. Guan, H. Yan, X.D. Cui, X.Y. Zhang, X. Li, H. Li, M. Cheng, Function of Kruppellike factor 2 in the shear stressinduced cell differentiation of endothelial progenitor cells to endothelial cells, Mol. Med. Rep. 19 (3) (2019) 1739–1746.
[37] S. SenBanerjee, Z. Lin, G.B. Atkins, D.M. Greif, R.M. Rao, A. Kumar, M.W. Feinberg, Z. Chen, D.I. Simon, F.W. Luscinskas, T.M. Michel, M.A. Gimbrone Jr., G. Garcia-Cardena, M.K. Jain, KLF2 Is a novel transcriptional regulator of endothelial proinflammatory activation, J. Exp. Med. 199 (10) (2004) 1305–1315.
[38] F.V. Sbrana, M. Cortini, S. Avnet, F. Perut, M. Columbaro, A. De Milito, N. Baldini, The role of autophagy in the maintenance of stemness and differentiation of mesenchymal stem cells, Stem Cell Rev. Rep. 12 (6) (2016) 621–633.
[39] S. Guixe-Muntet, F.C. de Mesquita, S. Vila, V. Hernandez-Gea, C. Peralta, J. C. Garcia-Pagan, J. Bosch, J. Gracia-Sancho, Cross-talk between autophagy and KLF2 determines endothelial cell phenotype and microvascular function in acute liver injury, J. Hepatol. 66 (1) (2017) 86–94.
[40] A. Parikh, C. Childress, K. Deitrick, Q.O. Lin, D. Rukstalis, W.N. Yang, Statin-induced autophagy by inhibition of geranylgeranyl biosynthesis in prostate cancer PC3 cells, Prostate 70 (9) (2010) 971–981.
[41] P.N. Hsieh, G.J. Zhou, Y.Y. Yuan, R.L. Zhang, D.A. Prosdocimo, P. Sangwung, A. H. Borton, E. Boriushkin, A. Hamik, H. Fujioka, C.E. Fealy, J.P. Kirwan, M. Peters, Y. Lu, X.D. Liao, D. Ramirez-Bergeron, Z.Y. Feng, M.K. Jain, A conserved KLF-autophagy pathway modulates nematode lifespan and mammalian age-associated vascular dysfunction, Nat. Commun. 8 (2017).
[42] Z. Hou, Z. Wang, Y. Tao, J. Bai, B. Yu, J. Shen, H. Sun, L. Xiao, Y. Xu, J. Zhou, Z. Wang, D. Geng, KLF2 regulates osteoblast differentiation by targeting of Runx2, Lab. Invest. 99 (2) (2019) 271–280.
[43] A. Briolay, P. Lencel, L. Bessueille, J. Caverzasio, R. Buchet, D. Magne, Autocrine stimulation of osteoblast activity by Wnt5a in response to TNF-alpha in human mesenchymal stem cells, Biochem. Biophys. Res. Commun. 430 (3) (2013) 1072–1077.
[44] V. Krishnan, H.U. Bryant, O.A. Macdougald, Regulation of bone mass by Wnt signaling, J. Clin. Invest. 116 (5) (2006) 1202–1209.
[45] E. Esen, J. Chen, C.M. Karner, A.L. Okunade, B.W. Patterson, F. Long, WNT-LRP5 signaling induces Warburg effect through mTORC2 activation during osteoblast differentiation, Cell Metabol. 17 (5) (2013) 745–755.
[46] E.J. Mackie, Osteoblasts: novel roles in orchestration of skeletal architecture, Int. J. Biochem. Cell Biol. 35 (9) (2003) 1301–1305.
[47] M. Zayzafoon, Calcium/calmodulin signaling controls osteoblast growth and differentiation, J. Cell. Biochem. 97 (1) (2006) 56–70.
[48] J. Gao, Z.H. Feng, X.Q. Wang, M.Q. Zeng, J. Liu, S.J. Han, J. Xu, L. Chen, K. Cao, J. G. Long, Z.F. Li, W.L. Shen, J.K. Liu, SIRT3/SOD2 maintains osteoblast differentiation and bone formation by regulating mitochondrial stress, Cell Death Differ. 25 (2) (2018) 229–240.
[49] J.H. Zhang, Autophagy and mitophagy in cellular damage control, Redox Biol. 1 (1) (2013) 19–23.
[50] R.J. Youle, A.M. van der Bliek, Mitochondrial fission, fusion, and stress, Science 337 (6098) (2012) 1062–1065.
[51] S.M. Jin, M. Lazarou, C. Wang, L.A. Kane, D.P. Narendra, R.J. Youle, Mitochondrial membrane potential regulates PINK1 import and proteolytic destabilization by PARL, J. Cell Biol. 191 (5) (2010) 933–942.
[52] R. Singh, A.M. Cuervo, Autophagy in the cellular energetic balance, Cell Metabol. 13 (5) (2011) 495–504.
[53] N. Shyh-Chang, H.H. Ng, The metabolic programming of stem cells, Genes Dev. 31 (4) (2017) 336–346.
[54] C.T. Chen, Y.R. Shih, T.K. Kuo, O.K. Lee, Y.H. Wei, Coordinated changes of mitochondrial biogenesis and antioxidant enzymes during osteogenic differentiation of human mesenchymal stem cells, Stem Cell. 26 (4) (2008) 960–968.
[55] S. Zhu, H. Wurdak, P.G. Schultz, Directed embryonic stem cell differentiation with small molecules, Future Med. Chem. 2 (6) (2010) 965–973.
[56] M.J. Birket, A.L. Orr, A.A. Gerencser, D.T. Madden, C. Vitelli, A. Swistowski, M. D. Brand, X. Zeng, A reduction in ATP demand and mitochondrial activity with neural differentiation of human embryonic stem cells, J. Cell Sci. 124 (Pt 3) (2011) 348–358.
[57] C.D. Folmes, T.J. Nelson, A. Martinez-Fernandez, D.K. Arrell, J.Z. Lindor, P. P. Dzeja, Y. Ikeda, C. Perez-Terzic, A. Terzic, Somatic oxidative bioenergetics transitions into pluripotency-dependent glycolysis to facilitate nuclear reprogramming, Cell Metabol. 14 (2) (2011) 264–271.
[58] M. Orgeur, M. Martens, G. Leonte, S. Nassari, M.A. Bonnin, S.T. Borno, B. Timmermann, J. Hecht, D. Duprez, S. Stricker, Genome-wide strategies identify downstream target genes of chick connective tissue-associated transcription factors, Development 145 (7) (2018).
[59] J. Ernst, P. Kheradpour, T.S. Mikkelsen, N. Shoresh, L.D. Ward, C.B. Epstein, X. L. Zhang, L. Wang, R. Issner, M. Coyne, M.C. Ku, T. Durham, M. Kellis, B. E. Bernstein, Mapping and analysis of chromatin state dynamics in nine human cell types, Nature 473 (7345) (2011) 43–U52.
[60] M.P. Creyghton, A.W. Cheng, G.G. Welstead, T. Kooistra, B.W. Carey, E.J. Steine, J. Hanna, M.A. Lodato, G.M. Frampton, P.A. Sharp, L.A. Boyer, R.A. Young, R. Jaenisch, Histone H3K27ac separates active from poised enhancers and predicts developmental state, Proc. Natl. Acad. Sci. U.S.A. 107 (50) (2010) 21931–21936.